An incremental flow theory for crystal plasticity incorporating strain gradient effects

Nellemann, Christopher; Niordson, Christian Frithiof; Nielsen, Kim Lau

Published in:
International Journal of Solids and Structures

Link to article, DOI:
10.1016/j.ijsolstr.2017.01.025

Publication date:
2017

Document Version
Peer reviewed version

An Incremental Flow Theory for Crystal Plasticity Incorporating Strain Gradient Effects

C. Nellemann[a,1,*], C.F. Niordson[a], K.L. Nielsen[a]

[a] *Department of Mechanical Engineering, Solid Mechanics, Technical University of Denmark, DK-2800 Kgs. Lyngby, Denmark*

Abstract

The present work investigates a new approach to formulating a rate-independent strain gradient theory for crystal plasticity. The approach takes as offset recent discussions published in the literature for isotropic plasticity, and a key ingredient of the present work is the manner in which a gradient enhanced effective slip measure governs hardening evolution. The effect of both plastic strains and plastic strain gradients are combined into this scalar effective slip quantity, the energy associated with plastic strain is dissipative (unrecoverable), while the energy from plastic strain gradients is recoverable (free). The framework developed forms the basis of a finite element implementation and is demonstrated on benchmark problems designed to bring out effects such as strengthening and hardening. Monotonic loading and plane strain deformation is assumed throughout, but despite this, non-proportional straining is predicted in the plastic regime even under pure shear conditions. Results of single slip and symmetric double slip reveal that strengthening and hardening are governed by the slip system orientation and the material length parameter only.

Keywords: Higher order theory, Size effects, Rate-independent formulation

*Corresponding author
Email address: chnel@mek.dtu.dk (C. Nellemann)
URL: http://orcid.org/0000-0002-9677-1285 (C. Nellemann)
[1]Tel: +45 4525-4263, Fax: +45 4593-1475

1. Introduction

Generalizations of plasticity theories, to account for strain gradient effects, have been discussed by a number of authors and approached in a variety of different ways. Common to the theories put forward by Fleck et al. (1994); Gudmundson (2004); Bardella (2006); Fleck and Willis (2009); Hutchinson (2012); Fleck et al. (2014, 2015) is that they include the effect of both plastic strain and their gradients through a combined plastic strain quantity, commonly referred to as an enhanced effective plastic strain and it was first suggested by Fleck et al. (1994) in the case of isotropic strain gradient plasticity. Despite originating from isotropic theory the effective strain measure has also taken root in the framework of strain gradient crystal plasticity, where it has been extended to describe the plastic strain state on individual slip systems (see e.g. Bardella, 2006; Borg, 2007). An attractive property of the effective plastic strain measure is that it incorporates strain gradient effects through a flow strength evolution law, as commonly done in conventional plasticity formulations through the plastic strains.

In an effort to characterize so-called strengthening and hardening Fleck et al. (2014) recently investigated the predictions of the theories put forward by Fleck and Willis (2009) and Hutchinson (2012). In the present work, strengthening is defined as an apparent delay in plastic flow, whereas hardening refers to the combined effect of both conventional strain hardening and hardening due to the presence of strain gradients. Fleck et al. (2015) extended the work on isotropic plasticity by Fleck et al. (2014), where it was found that strengthening characteristics are highly dependent on the effective strain measure and its relation to the plastic strain energy density. However, the issue of strain gradient related strengthening is not confined to isotropic strain gradient plasticity, but extends to theories of strain gradient crystal plasticity (e.g. Bardella, 2006; Gurtin et al., 2007).

The recent experimental evidence of a strengthening behavior in polycrystalline wires under cyclic loading has been reported by Liu et al. (2015), thus

highlighting the need for numerical models that incorporate such effects. The present work formulates a rate-independent strain gradient crystal plasticity theory which incorporates both strengthening and hardening. The formulation builds on the findings of Hutchinson (2012), mirroring a number of fundamental aspects of this isotropic strain gradient plasticity theory through the framework of strain gradient crystal plasticity formalized in Gurtin (2000, 2002). The objectives outlined in Hutchinson (2012) related to generalizing the conventional J_2-theory are adopted, but recast into the framework of crystal plasticity:

- The theory should reduce to the conventional crystal plasticity framework in the limit of sufficiently small slip gradients.
- In addition to elastic parameters, the input to the theory should be a relation between the resolved shear stress and the slip (a flow strength evolution curve) on the individual slip systems, $\tau_0^{(\alpha)}[\gamma_{eff}^{(\alpha)}]$, and a material length parameter, l, which characterizes the gradient dependence. The shear relation $\tau_0^{(\alpha)}[\gamma_{eff}^{(\alpha)}]$ is arbitrary, but monotonically increasing representing a hardening solid. As in conventional plasticity theory, latent hardening may be modeled through a latent hardening matrix, but it is omitted in the following.
- The flow theory and deformation theory must coincide for monotonic and proportional straining history.

The first objective implies that when relating the effective strain measure to a flow strength evolution curve the predictions of the new theory should equal the conventional crystal plasticity theory as $l \to 0$ (i.e. the effective plastic strain measure equals the conventional plastic strain measure in the limit of vanishing l). The second objective is fulfilled by relating the flow strength evolution on an individual slip system to the effective plastic strain measure. The presence of strain gradients increases the plastic work expended in the material, through the effective plastic strain measure, for the same amount of deformation. The third objective will not be substantiated in the present investigation because

a non-proportional straining history is predicted for the problem analyzed (see discussion in Section 5).

The effective plastic strain measure in the present formulation is defined in terms of both a dissipative and a recoverable contribution. Dissipation of plastic energy follows from the conventional crystal plasticity framework, while gradients of plastic strain are assumed to build up recoverable (free) energy in the material. The effective plastic strain defined in Hutchinson (2012) is formulated using the Mises equivalent strain measure in order to obtain a scalar quantity. However, the effective plastic strain measure in the present work is a scalar quantity defined on individual slip systems. Thus, a subtle difference in the definition of the strain gradient evolution exists between the formulation of Hutchinson (2012) and the present work.

For reasons highlighted in the presentation of the theory, the present framework will be restricted to an incremental version which is limited to monotonic loading. Model predictions for the case of pure shear loading of an infinite crystalline strip are used to illustrate key features of the theory.

The structure of the paper is as follows. In Section 2 the mathematical framework is presented. Section 3 presents the numerical discretization procedure and central aspects of the numerical implementation. In Section 4, the infinite crystalline strip problem is presented, while numerical predictions are displayed and discussed in Section 5. Strengthening and hardening predictions are investigated and compared to various models found in literature, both, isotropic strain gradient theory and strain gradient crystal plasticity theory. The results confirm the existence of strengthening for the present model, as predicted by Fleck et al. (2015) for a broader class of theories. Furthermore, both strengthening and hardening characteristics are quantifiable through their relation to the material length parameter. Finally, concluding remarks are given in Section 6.

2. Theoretical Framework

The general framework is presented in terms of flow theory characteristic in Section 2.1. The incremental formulation specialized to monotonic loading follows in Section 2.2. Index notation is adopted and indicated by subscript lowercase Latin letters. Superscript lowercase Greek letters define variables related to individual slip systems and a superscript (:) is used to indicate all active slip systems. Repeated lower case Latin indices imply summation, while comma separation implies spatial derivatives; $\frac{\partial}{\partial x_i} = ()_{,i}$. Incremental quantities representing a variables change with respect to a time like quantity (dimensionless parameter increasing monotonically with time) are indicated by $\dot{()}$, and functions will be indicated by the use of hard brackets e.g. $f[*]$.

2.1. General framework

The crystal plasticity framework describes an anisotropic material, with slip, $\gamma^{(\alpha)}$, occurring on a finite number of discrete slip systems. The α'th discrete crystallographic slip system is defined by a slip direction vector, $s_i^{(\alpha)}$, and a vector which is normal to the slip plane, $m_i^{(\alpha)}$. Both these vectors are of unit length. Thus, the macroscopic plastic strain, defined in terms of the total amount of slip occurring on all slip systems, is identified as

$$\varepsilon_{ij}^p = \sum_{(\alpha)} \gamma^{(\alpha)} \mu_{ij}^{(\alpha)}, \quad \text{with} \quad \mu_{ij}^{(\alpha)} = \frac{1}{2}\left(s_i^{(\alpha)} m_j^{(\alpha)} + s_j^{(\alpha)} m_i^{(\alpha)}\right) \tag{1}$$

with $\mu_{ij}^{(\alpha)}$ being the Schmid orientation tensor which relates the resolved shear stress, $\tau^{(\alpha)}$, to the Cauchy stress, σ_{ij}, through $\tau^{(\alpha)} = \sigma_{ij}\, \mu_{ij}^{(\alpha)}$.

The small strain measure defines the total strain $\varepsilon_{ij} = \left(u_{i,j} + u_{j,i}\right)/2$, through the spatial gradients of displacements $u_{i,j}$, with the displacements denoted by u_i. An additive decomposition of the total strain is adopted, with $\varepsilon_{ij} = \varepsilon_{ij}^e + \varepsilon_{ij}^p$, where ε_{ij}^e is the elastic strain.

The plastic response of the crystal is quantified phenomenologically through the density of all dislocations that accumulate during deformation - whether

the dislocations are statistically stored or geometrically necessary. Dissipation of energy is associated directly with the accumulation of statistically stored dislocations (SSDs), while geometrically necessary dislocations (GNDs) build up free energy. Inspired by incremental relations in the work of Bardella (2006) and Borg (2007) the gradient enhanced slip measure employed in the present work combine the slip and the spatial gradients of slip into the effective slip:

$$\gamma_{eff}^{(\alpha)} = \sqrt{\left(\gamma^{(\alpha)}\right)^2 + l^2 \left(\gamma_{,i}^{(\alpha)} s_i^{(\alpha)}\right)^2} \tag{2}$$

Here, l is a length parameter governing the gradient dependence of the material. The choice of equal length parameters for all crystallographic slip systems is based on the underlying assumption that gradient effects contribute equally to dissipation and recoverable energy on all slip systems. Furthermore, the choice of only accounting for the slip gradient along the slip direction, $\gamma_{,i}^{(\alpha)}\, s_i^{(\alpha)}$, implies that only pure edge dislocation densities are accounted for. There is no restriction on the sign of the slip increment (i.e. both positive and negative slip increments occur), thus; $\gamma^{(\alpha)} = \int_0^t \dot{\gamma}^{(\alpha)} \mathrm{d}t'$, while an accumulated slip measure is defined by; $\gamma_{acc}^{(\alpha)} = \int_0^t |\dot{\gamma}^{(\alpha)}| \mathrm{d}t'$, which is used to account for the total plastic slip throughout a general loading history. The choice of allowing both positive and negative slip increments obviously introduces a dependence on the sign of the slip increment, while the positive slip measure $|\gamma^{(\alpha)}|$ introduces a dependence on the sign of the slip in the mathematical formulation. Specifically the mathematical derivation in the present Section will rely on two derivatives, related to the evolution of the slip measures $|\gamma^{(\alpha)}|$ and $\gamma_{acc}^{(\alpha)}$, which are a direct consequence of considering both positive and negative slip increments. These are $\frac{\partial |\gamma^{(\alpha)}|}{\partial \gamma^{(\alpha)}} = \mathrm{sgn}[\gamma^{(\alpha)}]$, for $\gamma^{(\alpha)} \neq 0$ and $\frac{\partial \gamma_{acc}^{(\alpha)}}{\partial \gamma^{(\alpha)}} = \mathrm{sgn}[\dot{\gamma}^{(\alpha)}]$, for $\dot{\gamma}^{(\alpha)} \neq 0$, with $\mathrm{sgn}[*]$ denoting the sign function. The evolution of these slip measures and their derivatives are discussed in Appendix A, for the general loading case. The contribution from the slip gradient along the slip direction, $\gamma_{,i}^{(\alpha)}\, s_i^{(\alpha)}$, is assumed to be unrestricted with respect to sign, such that; $\gamma_{,i}^{(\alpha)} = \int_0^t \dot{\gamma}_{,i}^{(\alpha)} \mathrm{d}t'$. In the equivalent isotropic formulation defined by Hutchinson (2012), the gra-

dient contribution is defined with an absolute value operator, which would be expressed as; $\gamma^{(\alpha)}_{,i} = \int_0^t |\dot{\gamma}^{(\alpha)}|_{,i}\, \mathrm{d}t'$ in the present formulation.

The different slip measures presented above and their relation to the hardening relation assumed throughout the present work will be discussed in order to motivate the construction of a theory which applies to the case of general loading conditions. Thus, three cases will be used in this discussion, the case of monotonic and positive loading (i.e. deformation theory assuming that the slip occurs along the direction of the slip direction vector), the case of monotonic loading (i.e. deformation theory with slip occurring along the direction of the slip direction vector or the opposite direction) and the case of general loading (i.e. flow theory which accounts for history dependence). In the remainder of the present section, variables associated with the three cases will be indicated by a subscript $()_+$ for the case of monotonic and positive loading, $()_{+|-}$ for the case of monotonic loading and $()_{\leftrightarrow}$ for the case of general loading. Under monotonic loading, the effective slip incorporates the effects of SSD (since the contribution from the slip to the effective slip is always increasing) and GND associated energy, and a linear relation for the hardening curve is assumed

$$\tau_0^{(\alpha)}[\gamma^{(\alpha)}_{eff}] = \tau_y^{(\alpha)} \left(1 + k^{(\alpha)}\, \gamma^{(\alpha)}_{eff}\right) \tag{3}$$

This curve characterizes the critical resolved shear stress (slip resistance) $\tau_0^{(\alpha)}[\gamma^{(\alpha)}_{eff}]$ on the α'th slip system, through the initial slip resistance, $\tau_y^{(\alpha)}$ and the strength coefficient $k^{(\alpha)}$ (a schematic illustration is displayed in Fig. 1).

The work expended in the material is defined as the sum of the elastic and plastic energy contributions

$$U[\varepsilon^e_{ij}, \gamma^{(:)}, \gamma^{(:)}_{,i} s^{(:)}_i] = \frac{1}{2}\, L^e_{ijkl}\, \varepsilon^e_{kl}\, \varepsilon^e_{ij} + \sum_{(\alpha)} \left(\varphi^{(\alpha)} + \psi^{(\alpha)}\right) \tag{4}$$

where $L^e_{ijkl} = G\left((\delta_{ik}\delta_{jl} + \delta_{il}\delta_{jk}) + \frac{2\,\nu}{1-2\nu}\delta_{ij}\delta_{kl}\right)$ is the isotropic elastic stiffness tensor, G is the shear modulus, ν is Poisson's ratio, and δ_{ij} is the Kronecker

delta, while $\varphi^{(\alpha)}$ and $\psi^{(\alpha)}$ are dissipative and recoverable plastic energy contributions, respectively. In the case of monotonic loading the plastic contribution from the individual slip systems are defined by

$$\left(\varphi^{(\alpha)} + \psi^{(\alpha)}\right)_{+|-} = U^{p^{(\alpha)}}[\gamma_{eff}^{(\alpha)}] = \int_0^{\gamma_{eff}^{(\alpha)}} \tau_0^{(\alpha)}[\gamma']\mathrm{d}\gamma' \tag{5}$$

Thus, at a plastic deformation given by the slip $\gamma^{(\alpha)}$ and the net Burgers vector density $\gamma_{,i}^{(\alpha)}\, s_i^{(\alpha)}$, the plastic work expended in the material can be identified as the total area under the slip resistance curve in Fig. 1, satisfying the second objective defined in the introduction. From Eq. (5) it follows that the plastic energy reduces to that of the conventional crystal plasticity formulation; $\varphi_+^{(\alpha)} = U^{p^{(\alpha)}}[\gamma^{(\alpha)}] = \int_0^{\gamma^{(\alpha)}} \tau_0^{(\alpha)}[\gamma']\mathrm{d}\gamma'$, in the limit where gradients of slip are zero ($\gamma^{(\alpha)} = \gamma_{eff}^{(\alpha)}$, dark gray area in Fig. 1) assuming monotonic and positive loading. Thus, the plastic energy associated with gradients of slip can be identified by the plastic energy surplus (light gray area in Fig. 1):

$$\psi_+^{(\alpha)} = U^{p^{(\alpha)}}[\gamma_{eff}^{(\alpha)}] - U^{p^{(\alpha)}}[\gamma^{(\alpha)}] = \int_{\gamma^{(\alpha)}}^{\gamma_{eff}^{(\alpha)}} \tau_0^{(\alpha)}[\gamma']\mathrm{d}\gamma' \tag{6}$$

A given level of plastic work can be reached in two ways. In the absence of strain gradients the measure $\gamma_{eff}^{(\alpha)} = \gamma^{(\alpha)}$ will give rise to a certain level of plastic work, which can also be reached in the presence of strain gradients, however, at a lower $\gamma^{(\alpha)}$ due to the gradient contribution to $\gamma_{eff}^{(\alpha)}$, consistent with the notion that GNDs account for the difference in plastic work between $\gamma^{(\alpha)}$ and $\gamma_{eff}^{(\alpha)}$. The plastic energy contribution given by Eq. (5) is valid for the case of monotonic loading since the effective slip measure essentially accounts for the absolute value of the slip, which is not the case for $\varphi_+^{(\alpha)}$. Thus, to account for monotonic negative loading the conventional limit of the plastic energy contribution is given by $\varphi_{+|-}^{(\alpha)} = U^{p^{(\alpha)}}[|\gamma^{(\alpha)}|] = \int_0^{|\gamma^{(\alpha)}|} \tau_0^{(\alpha)}[\gamma']\mathrm{d}\gamma'$, which results in the plastic energy associated with gradient of slip in the case of monotonic loading

$$\psi_{+|-}^{(\alpha)} = U^{p^{(\alpha)}}[\gamma_{eff}^{(\alpha)}] - U^{p^{(\alpha)}}[|\gamma^{(\alpha)}|] = \int_{|\gamma^{(\alpha)}|}^{\gamma_{eff}^{(\alpha)}} \tau_0^{(\alpha)}[\gamma']\mathrm{d}\gamma' \tag{7}$$

This energy surplus is by definition, in the present model, a recoverable energy contribution, such that Eq. (7) is also valid in the case of general loading ($\psi^{(\alpha)}_{\leftrightarrow} = \psi^{(\alpha)}_{+|-}$). Furthermore, the conventional limit of the plastic energy contribution in the case of general loading must include history dependence beyond that of the recoverable energy contribution (i.e. account for slip even if the recoverable energy contribution builds up and decreases back to zero). Thus, in the case of general loading the conventional limit of the plastic energy contribution must depend on the accumulated slip as $\varphi^{(\alpha)}_{\leftrightarrow} = U^{p^{(\alpha)}}[\gamma^{(\alpha)}_{acc}] = \int_0^{\gamma^{(\alpha)}_{acc}} \tau^{(\alpha)}_0[\gamma']\mathrm{d}\gamma'$.

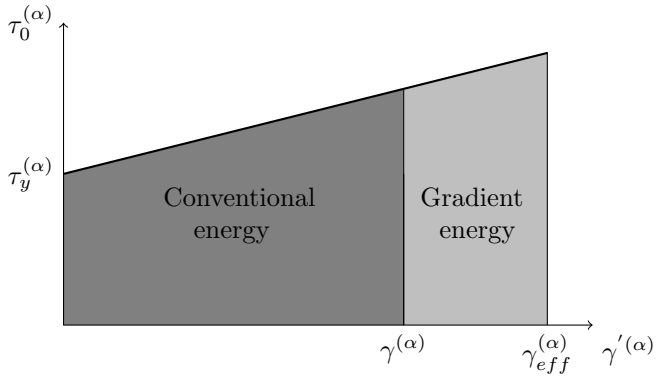

Figure 1: Illustration of the slip resistance, $\tau_0^{(\alpha)}$, as a function of slip, at a monotonically increasing and positive load resulting in the plastic deformation given by $\gamma^{(\alpha)}$ and net Burgers vector density $\gamma^{(\alpha)}_{,i}\, s^{(\alpha)}_i$. Initial yield has occurred on slip system "α" when the resolved shear stress reached the value of $\tau_y^{(\alpha)}$. The crystallographic slip, $\gamma^{(\alpha)}$, contributes to a conventional energy (dark gray), while additional recoverable energy (light gray) is stored in the presence of strain gradients through the effective slip, $\gamma^{(\alpha)}_{eff}$ $\left(\gamma^{(\alpha)} \leq \gamma^{(\alpha)}_{eff}\right)$.

The general framework for strain gradient crystal plasticity proposed by Gurtin (2000) will serve as a basis for the remainder of the derivation. Thus, the incremental strain energy density can be defined in terms of strain quantities and their work conjugate stress quantities by

$$\begin{aligned}\dot{U}[\varepsilon^e_{ij},\gamma^{(:)},\gamma^{(:)}_{,i}s^{(:)}_i] &= \sigma_{ij}\dot{\varepsilon}^e_{ij}+\sum_{(\alpha)}\left(\overbrace{\frac{\partial U^{p^{(\alpha)}}[\gamma^{(\alpha)}_{eff},\gamma^{(\alpha)}_{acc}]}{\partial\gamma^{(\alpha)}}}^{q^{(\alpha)}}\frac{\partial\gamma^{(\alpha)}}{\partial t}+\overbrace{\frac{\partial U^{p^{(\alpha)}}[\gamma^{(\alpha)}_{eff},\gamma^{(\alpha)}_{acc}]}{\partial\left(\gamma^{(\alpha)}_{,i}s^{(\alpha)}_i\right)}}^{\xi^{(\alpha)}}\frac{\partial\left(\gamma^{(\alpha)}_{,i}s^{(\alpha)}_i\right)}{\partial t}\right)\\ &= \sigma_{ij}\dot{\varepsilon}^e_{ij}+\sum_{(\alpha)}\left(q^{(\alpha)}\dot{\gamma}^{(\alpha)}+\xi^{(\alpha)}\dot{\gamma}^{(\alpha)}_{,i}s^{(\alpha)}_i\right)\end{aligned}\tag{8}$$

The strong form of the equilibrium equations are (see Gurtin, 2000)

$$\sigma_{ij,j} = 0 \tag{9}$$

$$q^{(\alpha)}-\tau^{(\alpha)}-\xi^{(\alpha)}_{,i}s^{(\alpha)}_i = 0 \tag{10}$$

Here, $q^{(\alpha)}$ is the micro-stress, work conjugate to the slip, and $\xi^{(\alpha)}$ is the higher order stress, work conjugate to the net Burgers vector density $\gamma^{(\alpha)}_{,i}\,s^{(\alpha)}_i$.

The Cauchy stress is work conjugate to the elastic strain and is given by the conventional relation

$$\sigma_{ij} = \frac{\partial U}{\partial\varepsilon^e_{ij}} = L^e_{ijkl}\varepsilon^e_{kl} \tag{11}$$

The micro-stress for each slip system can be derived by $q^{(\alpha)}=\frac{\partial U}{\partial\gamma^{(\alpha)}}$ and it is additively decomposed into a recoverable and a dissipative part as $q^{(\alpha)}=q^{R(\alpha)}+q^{D(\alpha)}$. In the case of monotonic and positive loading the recoverable micro-stress is $q^{R(\alpha)}=\frac{\partial\psi^{(\alpha)}_+}{\partial\gamma^{(\alpha)}}$ while it is

$$q^{R(\alpha)} = \frac{\partial\psi^{(\alpha)}_{\leftrightarrow}}{\partial\gamma^{(\alpha)}} = \left(\tau^{(\alpha)}_0[\gamma^{(\alpha)}_{eff}]\frac{\gamma^{(\alpha)}}{\gamma^{(\alpha)}_{eff}}-\tau^{(\alpha)}_0[|\gamma^{(\alpha)}|]\,\mathrm{sgn}[\gamma^{(\alpha)}]\right) \tag{12}$$

in the case of general loading. In the case of monotonic and positive loading the dissipative micro-stress is $q^{D(\alpha)}=\frac{\partial\varphi^{(\alpha)}_+}{\partial\gamma^{(\alpha)}}$, in the case of monotonic loading it is $q^{D(\alpha)}=\frac{\partial\varphi^{(\alpha)}_{+|-}}{\partial\gamma^{(\alpha)}}$ while it is

$$q^{D(\alpha)} = \frac{\partial \varphi^{(\alpha)}_{\leftrightarrow}}{\partial \gamma^{(\alpha)}} = \tau_0^{(\alpha)}[\gamma^{(\alpha)}_{acc}]\,\mathrm{sgn}[\dot{\gamma}^{(\alpha)}] \quad \text{for} \quad \dot{\gamma}^{(\alpha)} \neq 0 \tag{13}$$

in the case of general loading. The latter ensures positive dissipation of energy since the dissipative stress quantity has the same sign as the slip increment ($q^{D(\alpha)}\dot{\gamma}^{(\alpha)} \geq 0$) and it includes a dependence on the total slip history. An implication of this expression is that the dissipative micro-stress may vary discontinuously with $\mathrm{sgn}[\dot{\gamma}^{(\alpha)}]$. The recoverable micro-stress, $q^{R(\alpha)}$, has the same sign as $\gamma^{(\alpha)}$, such that the recoverable energy, $q^{R(\alpha)}\gamma^{(\alpha)}$, is a positive quantity which increases or decreases with the value of $|\gamma^{(\alpha)}|$ and $\gamma^{(\alpha)}_{eff}$. Thus, the micro-stress under general loading conditions is $\frac{\partial U}{\partial \gamma^{(\alpha)}} = \frac{\partial \psi^{(\alpha)}_{\leftrightarrow}}{\partial \gamma^{(\alpha)}} + \frac{\partial \varphi^{(\alpha)}_{\leftrightarrow}}{\partial \gamma^{(\alpha)}}$:

$$q^{(\alpha)} = \overbrace{\tau_0^{(\alpha)}[\gamma^{(\alpha)}_{eff}]\frac{\gamma^{(\alpha)}}{\gamma^{(\alpha)}_{eff}} - \tau_0^{(\alpha)}[|\gamma^{(\alpha)}|]\,\mathrm{sgn}[\gamma^{(\alpha)}]}^{q^{R(\alpha)}} + \overbrace{\tau_0^{(\alpha)}[\gamma^{(\alpha)}_{acc}]\,\mathrm{sgn}[\dot{\gamma}^{(\alpha)}]}^{q^{D(\alpha)}} \quad \text{for} \quad \dot{\gamma}^{(\alpha)} \neq 0 \quad \text{and} \quad \gamma^{(\alpha)} \neq 0 \tag{14}$$

which describes the plastic energy evolution sketched in Fig. 1 under monotonic loading ($|\gamma^{(\alpha)}| = \gamma^{(\alpha)}_{acc}$ and $\mathrm{sgn}[\dot{\gamma}^{(\alpha)}] = \mathrm{sgn}[\gamma^{(\alpha)}]$). Moreover, the dissipative micro-stress expression accounts for the build up of plastic strains under general loading conditions, through the accumulated slip, consistent with the accumulation of SSD associated energy.

The higher order stress is defined as $\xi^{(\alpha)} = \frac{\partial U}{\partial\left(\gamma^{(\alpha)}_{,i} s^{(\alpha)}_i\right)}$, such that

$$\xi^{(\alpha)} = \frac{\partial \psi^{(\alpha)}_{\leftrightarrow}}{\partial\left(\gamma^{(\alpha)}_{,i} s^{(\alpha)}_i\right)} = \tau_0^{(\alpha)}[\gamma^{(\alpha)}_{eff}]\, l^2\, \frac{\gamma^{(\alpha)}_{,i} s^{(\alpha)}_i}{\gamma^{(\alpha)}_{eff}} \tag{15}$$

In the limit $l \to 0$, no gradient dependence exists and the conventional crystal plasticity formulation is recovered, with Eq. (10) simplifying to $q^{(\alpha)} = q^{D(\alpha)} = \tau^{(\alpha)}$ (satisfying the first objective defined in the introduction). In the

present formulation, the gradient dependence is introduced through the recoverable micro-stress contribution and the higher order stress, which must both exist to fulfill the higher order equilibrium equation (see Eq. (10)). Furthermore, while this quantity is termed recoverable energy, actual recovery may not, in general, be possible through mechanical deformation, but the energy is in principle available through an annealing process.

2.2. Incremental formulation assuming monotonic loading

In this section, the strain gradient crystal plasticity framework is cast into incremental form, however, restricted to monotonic loading history. Thus, $|\gamma^{(\alpha)}| = \gamma^{(\alpha)}_{acc}$ and $\text{sgn}[\dot{\gamma}^{(\alpha)}] = \text{sgn}[\gamma^{(\alpha)}]$. This restriction is chosen purely to simplify the discussion, preserving only the key characteristics relevant to the investigation of the present work. The incremental increase of SSDs is associated with $\dot{\gamma}^{(\alpha)}_{acc} = \dot{\gamma}^{(\alpha)}$, while the incremental increase of GNDs is associated with the increment of the net Burgers vector density $\dot{\gamma}^{(\alpha)}_{,i}\, s^{(\alpha)}_i$. Following the definition of the effective slip (Eq. (2)) the increment of the effective slip takes the form

$$\dot{\gamma}^{(\alpha)}_{eff} \;=\; \frac{\dot{\gamma}^{(\alpha)}\gamma^{(\alpha)} + l^2\, \gamma^{(\alpha)}_{,i}\, s^{(\alpha)}_i\, \dot{\gamma}^{(\alpha)}_{,j}\, s^{(\alpha)}_j}{\gamma^{(\alpha)}_{eff}} \tag{16}$$

Increments of the strain quantities follow directly, such that the increments of total strain are given in terms of increments of displacement gradients, $\dot{\varepsilon}_{ij} = \frac{1}{2}\left(\dot{u}_{i,j} + \dot{u}_{j,i}\right)$, additively decomposed into elastic, $\dot{\varepsilon}^e_{ij}$, and plastic, $\dot{\varepsilon}^p_{ij}$, components, $\dot{\varepsilon}_{ij} = \dot{\varepsilon}^e_{ij} + \dot{\varepsilon}^p_{ij}$, with the plastic components given by, $\dot{\varepsilon}^p_{ij} = \sum_{(\alpha)} \dot{\gamma}^{(\alpha)} \mu^{(\alpha)}_{ij}$. The elastic relation defines the conventional stress increments as follows

$$\dot{\sigma}_{ij} \;=\; L^e_{ijkl}\left(\dot{\varepsilon}_{kl} - \sum_{(\beta)} \dot{\gamma}^{(\beta)} \mu^{(\beta)}_{kl}\right) \tag{17}$$

The increment of resolved shear stress is given by $\dot{\tau}^{(\alpha)} = \dot{\sigma}_{ij}\mu^{(\alpha)}_{ij}$. The micro-stress defined in Eq. (14) reduces to; $q^{(\alpha)} = \frac{\partial \varphi^{(\alpha)}_{+|-}}{\partial \gamma^{(\alpha)}} + \frac{\partial \psi^{(\alpha)}_{+|-}}{\partial \gamma^{(\alpha)}} = \tau^{(\alpha)}_0[\gamma^{(\alpha)}_{eff}]\frac{\gamma^{(\alpha)}}{\gamma^{(\alpha)}_{eff}}$ under monotonic loading, and thus, the incremental micro-stress is given by

$$\dot{q}^{(\alpha)} \quad = \quad h^{(\alpha)}[\gamma_{eff}^{(\alpha)}]\dot{\gamma}_{eff}^{(\alpha)}\frac{\gamma^{(\alpha)}}{\gamma_{eff}^{(\alpha)}} + \tau_0^{(\alpha)}[\gamma_{eff}^{(\alpha)}]\left(\frac{\dot{\gamma}^{(\alpha)}}{\gamma_{eff}^{(\alpha)}} - \dot{\gamma}_{eff}^{(\alpha)}\frac{\gamma^{(\alpha)}}{\gamma_{eff}^{(\alpha)^2}}\right) \tag{18}$$

Here, the hardening moduli defined by $h^{(\alpha)}[\gamma_{eff}^{(\alpha)}] = \frac{\partial \tau_0^{(\alpha)}[\gamma_{eff}^{(\alpha)}]}{\partial \gamma_{eff}^{(\alpha)}}$ only accounts for self-hardening, neglecting the effects of latent hardening. The incremental slip resistance follows from the differentiation of Eq. (3) as; $\dot{\tau}_0^{(\alpha)} = h^{(\alpha)}[\gamma_{eff}^{(\alpha)}]\,\dot{\gamma}_{eff}^{(\alpha)}$, which can be identified as part of the first term in Eq. (18).

The incremental higher order stress follows from Eq. (15) and is given by

$$\dot{\xi}^{(\alpha)} \quad = \quad l^2 s_i^{(\alpha)}\left(h^{(\alpha)}[\gamma_{eff}^{(\alpha)}]\dot{\gamma}_{eff}^{(\alpha)}\frac{\gamma_{,i}^{(\alpha)}}{\gamma_{eff}^{(\alpha)}} + \tau_0^{(\alpha)}[\gamma_{eff}^{(\alpha)}]\left(\frac{\dot{\gamma}_{,i}^{(\alpha)}}{\gamma_{eff}^{(\alpha)}} - \dot{\gamma}_{eff}^{(\alpha)}\frac{\gamma_{,i}^{(\alpha)}}{\gamma_{eff}^{(\alpha)^2}}\right)\right) \tag{19}$$

The principle of virtual work, on incremental form, for a body with volume V and surface S is given by

$$\int_V \left(\dot{\sigma}_{ij}\delta\dot{\varepsilon}_{ij} + \sum_{(\alpha)}\left(\dot{q}^{(\alpha)} - \dot{\tau}^{(\alpha)}\right)\delta\dot{\gamma}^{(\alpha)} + \sum_{(\alpha)}\dot{\xi}^{(\alpha)}s_i^{(\alpha)}\delta\dot{\gamma}_{,i}^{(\alpha)}\right)\mathrm{d}V = \int_S\left(\dot{T}_i\delta\dot{u}_i + \sum_{(\alpha)}\dot{r}^{(\alpha)}\delta\dot{\gamma}^{(\alpha)}\right)\mathrm{d}S \tag{20}$$

Here, δ refers to a variational quantity, $\dot{T}_i$ represents the increments of the surface tractions, work conjugate to displacements, and $\dot{r}^{(\alpha)}$ represents the increments of higher order tractions, work conjugate to slips. The tractions on the boundaries are given by; $\dot{T}_i = \dot{\sigma}_{ij}\,n_j$ and $\dot{r}^{(\alpha)} = \dot{\xi}^{(\alpha)}\,s_j^{(\alpha)}\,n_j$, with n_j being the outward unit normal.

The assumption of monotonic loading simplifies the numerical solution procedure, when based on the finite element method, as it excludes the need for evaluation of elastic unloading. However, a yield criterion is still needed. As discussed by Hutchinson (2012), in relation to isotropic plasticity, only the Cauchy stress, σ_{ij}, is assumed to change during elastic deformation. Thus, initial yield

on the α'th slip system is in the present work defined as in the case of conventional crystal plasticity when $\tau^{(\alpha)} = \tau_0^{(\alpha)}[0] = \tau_y^{(\alpha)}$.

3. Numerical Method

The mathematical notation in this section relies on superscript upper-case Latin letters that identify elements in one and two-dimensional arrays, except the letter T which is used to indicate the transpose of a matrix.

3.1. Finite element discretization

The numerical formulation follows from the discretization of Eq. (20), where increments of displacement and increments of slip are free variables. The variational quantities and field quantities are discretized using polynomial interpolation functions. In this case, a plane strain formulation is employed, with 8 node quadratic isoparametric elements used to discretize displacement associated quantities. Thus, the shape functions N_i^M are used to interpolate increments of nodal displacements, $\dot{d}^M$, such that a total of 16 shape functions are used to approximate increments of displacements and increments of strains in two dimensions

$$\dot{u}_i = \sum_{M=1}^{16} N_i^M \, \dot{d}^M \quad \text{and} \quad \dot{\varepsilon}_{ij} = \sum_{M=1}^{16} E_{ij}^M \, \dot{d}^M \tag{21}$$

Here, $E_{ij}^M = \frac{1}{2}(N_{i,j}^M + N_{j,i}^M)$ is the strain-displacement matrix. The slip quantities are discretized by 4 node bilinear elements using isoparametric shape functions M^N, and their derivatives $M_{,i}^N$. Thus, a total of 4 shape functions are used to approximate increments of slip and their spatial gradients from the nodal slips, $\dot{g}^{(\alpha)N}$, as

$$\dot{\gamma}^{(\alpha)} = \sum_{N=1}^{4} M^{(\alpha)N} \, \dot{g}^{(\alpha)N} \quad \text{and} \quad \dot{\gamma}_{,i}^{(\alpha)} = \sum_{N=1}^{4} M_{,i}^{(\alpha)N} \, \dot{g}^{(\alpha)N} \tag{22}$$

Discretization of Eq. (20) results in a system of equations which takes the form

$$\begin{bmatrix} \left[K_e\right] & \left[K_{ep}^{(\alpha)}\right] \\ \left[K_{ep}^{(\alpha)}\right]^T & \left[K_p^{(\alpha,\beta)}\right] \end{bmatrix} \begin{Bmatrix} \left\{\dot{d}\right\} \\ \left\{\dot{g}^{(\alpha)}\right\} \end{Bmatrix} = \begin{Bmatrix} \left\{F_1\right\} \\ \left\{F_2^{(\alpha)}\right\} \end{Bmatrix} \tag{23}$$

with the three matrices $\left[K_e\right]$, $\left[K_{ep}^{(\alpha)}\right]$ and $\left[K_p^{(\alpha,\beta)}\right]$ identified as

(i) The conventional elastic stiffness matrix

$$\left[K_e\right]^{MN} = \int_V L_{ijkl}^e E_{kl}^M E_{ij}^N \mathrm{d}V \tag{24}$$

(ii) Elastic-plastic matrices which couple nodal increments of displacements and nodal increments of slip

$$\left[K_{ep}^{(\alpha)}\right]^{MN} = -\sum_{(\alpha)} \int_V L_{ijkl}^e \mu_{kl}^{(\alpha)} M^{(\alpha)M} E_{ij}^N \mathrm{d}V \tag{25}$$

(iii) Slip system matrices which couple nodal increments of slip, either on an individual slip system ($\alpha = \beta$) or across two distinct slip systems ($\alpha \neq \beta$)

$$\begin{aligned}
\left[K_p^{(\alpha,\beta)}\right]^{MN} &= \sum_{(\alpha)} \sum_{(\beta)} \left(\int_V \mu_{ij}^{(\alpha)} L_{ijkl}^e \mu_{kl}^{(\beta)} M^{(\beta)M} M^{(\alpha)N} \mathrm{d}V \right. \\
&+ \delta_{\alpha\beta} \int_V \left(\left(\left(h^{(\alpha)}[\gamma_{eff}^{(\alpha)}] - \frac{\tau_0^{(\alpha)}[\gamma_{eff}^{(\alpha)}]}{\gamma_{eff}^{(\alpha)}} \right) \frac{\gamma^{(\alpha)^2}}{\gamma_{eff}^{(\alpha)^2}} + \frac{\tau_0^{(\alpha)}[\gamma_{eff}^{(\alpha)}]}{\gamma_{eff}^{(\alpha)}} \right) M^{(\alpha)M} M^{(\alpha)N} \right) \mathrm{d}V \\
&+ \delta_{\alpha\beta} \int_V \left(h^{(\alpha)}[\gamma_{eff}^{(\alpha)}] - \frac{\tau_0^{(\alpha)}[\gamma_{eff}^{(\alpha)}]}{\gamma_{eff}^{(\alpha)}} \right) \frac{\gamma^{(\alpha)}}{\gamma_{eff}^{(\alpha)^2}} l^2 \gamma_{,i}^{(\alpha)} s_i^{(\alpha)} s_j^{(\alpha)} M_{,j}^{(\alpha)M} M^{(\alpha)N} \mathrm{d}V \\
&+ \delta_{\alpha\beta} \int_V \left(h^{(\alpha)}[\gamma_{eff}^{(\alpha)}] - \frac{\tau_0^{(\alpha)}[\gamma_{eff}^{(\alpha)}]}{\gamma_{eff}^{(\alpha)}} \right) \frac{\gamma^{(\alpha)}}{\gamma_{eff}^{(\alpha)^2}} l^2 \gamma_{,i}^{(\alpha)} s_i^{(\alpha)} M^{(\alpha)M} s_j^{(\alpha)} M_{,j}^{(\alpha)N} \mathrm{d}V \\
&+ \delta_{\alpha\beta} \int_V \left(\left(h^{(\alpha)}[\gamma_{eff}^{(\alpha)}] - \frac{\tau_0^{(\alpha)}[\gamma_{eff}^{(\alpha)}]}{\gamma_{eff}^{(\alpha)}} \right) \frac{\left(l^2 \gamma_{,i}^{(\alpha)} s_i^{(\alpha)} \right)^2}{\gamma_{eff}^{(\alpha)^2}} + l^2 \frac{\tau_0^{(\alpha)}[\gamma_{eff}^{(\alpha)}]}{\gamma_{eff}^{(\alpha)}} \right) s_j^{(\alpha)} M_{,j}^{(\alpha)M} s_k^{(\alpha)} M_{,k}^{(\alpha)N} \mathrm{d}V \Bigg)
\end{aligned} \tag{26}$$

The right-hand side of Eq. (23) contains two contributions; $\left\{F_1\right\}$ related to conventional tractions, and $\left\{F_2^{(\alpha)}\right\}$ related to higher order tractions. These are defined by

$$\{F_1\}^N = \int_S \dot{T}_i N_i^N \mathrm{d}S \tag{27}$$

$$\left\{F_2^{(\alpha)}\right\}^N = \sum_{(\alpha)} \int_S \dot{r}^{(\alpha)} M^{(\alpha)N} \mathrm{d}S \tag{28}$$

In the case of single slip ($\alpha = \beta = 1$), the combined element matrix in Eq. (23) comprises of; (i) the elastic stiffness matrix (16 x 16 in size), (ii) the elastic-plastic coupling matrix (4 x 16), and (iii) the slip system matrix (4 x 4). In the case of multiple active slip systems, additional coupling matrices appear, compared to the case of single slip, and the combined element matrix in Eq. (23) then comprises of additional; (ii) elastic-plastic coupling matrices and (iii) slip system coupling matrices. Correspondingly, 4 additional nodal slip variables and 4 additional right-hand side components appear for each additional slip system.

3.2. Numerical implementation

The discretized equations have been implemented into an in-house finite element code. Numerical integration follows the conventional Gauss quadrature rule. Full integration of the 8 node element implies 3×3 Gauss points, which is also used for the 4 node element.

Evaluation of initial yield is carried out on Gauss point basis, such that the element stiffness may consist of both elastic and elastic-plastic contributions. In non-active plastic Gauss points, $\left[K_{ep}^{(\alpha)}\right]$ and $\left[K_p^{(\alpha,\beta)}\right]$ are set equal to zero when evaluating the combined element stiffness matrix. However, if a slip system is inactive in all Gauss points belonging to a specific element the stiffness matrix contributions from $\left[K_p^{(\alpha,\beta)}\right]$, for $\alpha = \beta$, are set equal to the identity matrix multiplied by a sufficiently large value (in the present work $10^7 \times G$). This procedure is essentially a penalty method approach ensuring no slip on elements

where a slip system is inactive.

Special attention should be paid to several terms of Eq. (26) because of their singular nature at initial yield. The approach chosen to overcome this numerical issue is to start calculations with a small value of initial slip throughout the analyzed body. The effect of this initial starting value on the final solution is investigated in Appendix B. For completeness, it is noted that the finite element implementation utilizes the external package SuiteSparse (Davis et al., 2014) through the framework PETSc (Balay et al., 2015) for solving the sparse linear system of equations.

4. Problem formulation

Investigation of the model predictions is carried out by examining an infinite strip of crystalline material, which is sandwiched between rigid platens. The strip is subjected to monotonic pure shear loading conditions under the assumption of plane strain deformation. A crystalline strip of height H and width W is sketched in Fig. 2. The sketch describes a material with two slip systems inclined by the angle $\theta^{(1)} = -\theta^{(2)} = \theta$, with respect to the x_1-axis. In terms of conventional boundary conditions the pure shear problem is constrained, in the direction parallel to the x_2-axis, on the entire boundary ($u_2 = 0$ on $x_2 = \pm H/2$ and $x_1 = \pm W/2$). Prescribed displacements, $\Delta/2$, act in opposite directions parallel to the x_1-axis, on $x_2 = \pm H/2$, such that $u_1 = \Delta x_2/H = \pm\Delta/2$. Periodicity of displacements is prescribed on $x_1 = \pm W/2$, with respect the x_2-coordinate ($u_1[-W/2, x_2] = u_1[W/2, x_2]$). Higher order boundary conditions consist of micro-hard boundaries enforced on $x_2 = \pm H/2$: $\gamma^{(\alpha)} = 0$ for $l > 0$. Furthermore, periodicity of the slip is enforced on $x_1 = \pm W/2$: $\gamma^{(\alpha)}[-W/2, x_2] = \gamma^{(\alpha)}[W/2, x_2]$. The shear load increment is monotonically prescribed in steps of equal amplitude. A single column of 1000 square elements over the height H is used to obtain results, and the load is prescribed in 10000 displacement increments in order to ensure convergence of the solution.

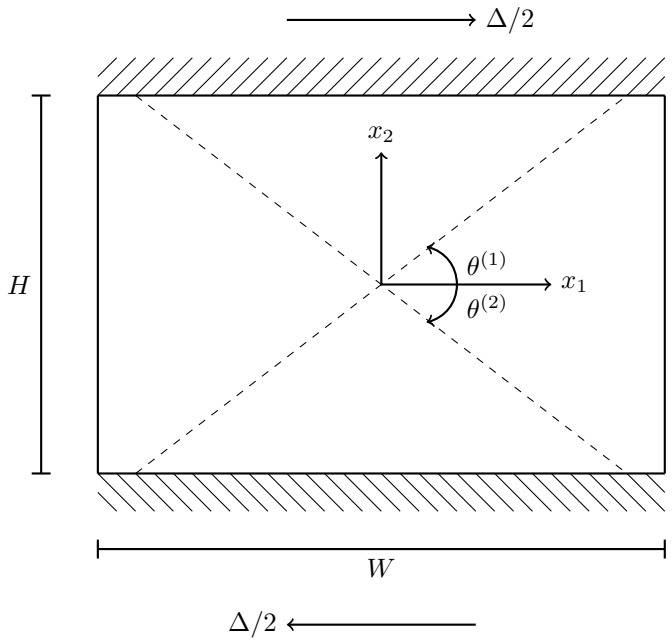

Figure 2: Illustration of a crystalline strip of height H and width W subjected to pure shear loading conditions. The material is elastic-plastic, with two slip systems (indicated by dashed lines) inclined by the angle $\theta^{(1)} = -\theta^{(2)} = \theta$ with respect to the x_1-axis. Micro-hard boundary conditions, blocking the motion of dislocations, are applied onto the top and the bottom of the strip, which are displaced the distance $\Delta/2$ in the horizontal direction (indicated by arrows).

The material is characterized by the ratio of the yield stress to the shear modulus $\tau_y/G = 0.0104$. The value of the normalized conventional strain hardening parameter is $h/G = 0.2$, unless otherwise stated. Furthermore, a reference strain measure, γ_y, is defined in terms of the initial yield stress through $\tau_y = G\,\gamma_y$.

Both single slip (in this case $\theta = 90°$) and symmetric double slip ($\theta = 15°$ and $30°$, respectively) will be investigated in Section 5. The Cauchy stress components $\sigma_{12} = \sigma_{21}$ are the only nonvanishing conventional stress components for these configurations of slip systems and boundary conditions. Essentially this problem is a one dimensional boundary value problem for the slip variables and the horizontal displacements, given in terms of the constant resolved shear stress imposed on the strip (see Bittencourt et al., 2003, for details).

5. Results and discussion

Different terminology is used in the literature when defining plastic flow characteristics. In the present work, strengthening is defined as an apparent delay in plastic flow, whereas hardening refers to the combined effect of both conventional strain hardening and hardening due to the presence of strain gradients. It is noted that strengthening behavior associated with the present theory arises due to a delay in plastic flow predictions beyond the initial yield stress, as discussed by Fleck et al. (2015) in the case of rate-independent isotropic strain gradient plasticity theory.

From here on all parameters related to plasticity are presented without superscript Greek letter slip system identifier since both are assumed equal in the case of symmetric double slip and only one exists in the case of single slip. The distinction between individual parameters for several slip system orientations are presented by the use of a subscript θ, representing the different slip system orientation angles.

5.1. Single slip

Model predictions for the case of single slip, with the slip system orientation angle specified by $\theta = 90^\circ$, are presented in Figs. 3 - 9. The resolved shear stress response for varying values of the normalized length parameter l/H is shown in Fig. 3, for several values of l/H from 0 to 1.6. The results reveal both increased strengthening and increased hardening for increasing values of l/H, while the conventional limit is obtained as $l/H \to 0$. Furthermore, in spite of the prescribed linear strain hardening a slight curvature of the response curves is seen for $l/H > 0$, and this effect becomes more evident as l/H increases. Figure 4 presents the slip profile amplitude as a function of overall shear strain Δ/H. The relationship between the amplitude and the overall shear strain is non-linear in the plastic regime for values of $l/H > 0$ and this non-linearity increases with l/H. The non-linear relationship is an indication of a non-proportional straining history, as discussed by Hutchinson (2012).

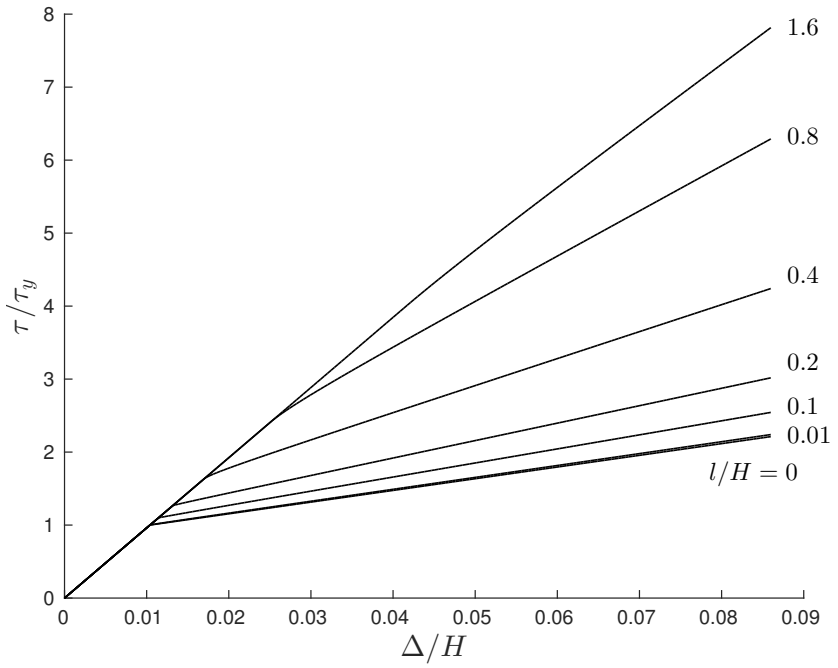

Figure 3: Normalized resolved shear stress to the imposed overall shear strain Δ/H for single slip ($\theta = 90°$), for various values of the normalized length parameter l/H. The normalized conventional strain hardening parameter is $h/G = 0.2$.

Figure 5 shows the predictions of the slip at the final stage of deformation. The results clearly reflect the presence of strain gradients, both in the sense of a non-uniform slip profile distribution and in the sense of an overall decrease in slip profile amplitude due to increased hardening for increasing values of l/H. Furthermore, a distinct change in profile shape is predicted as l/H becomes small but larger than zero, with an almost uniform slip distribution predicted through most of the strip height. In the limit, the slip profile converges to that of the conventional material response where the gradient terms disappear and the micro-hard boundary condition can not be enforced (Bittencourt et al., 2003). The normalized net Burgers vector density, $l\,\gamma_{,2}\,s_2$, predictions associated with the slip profiles of Fig. 5 are shown in Fig. 6. The result obtained for $l/H = 0.01$ shows a highly localized distribution at the boundaries, whereas the curves for values between 0.1 and 0.4 predict a decreasing localization of the distribution.

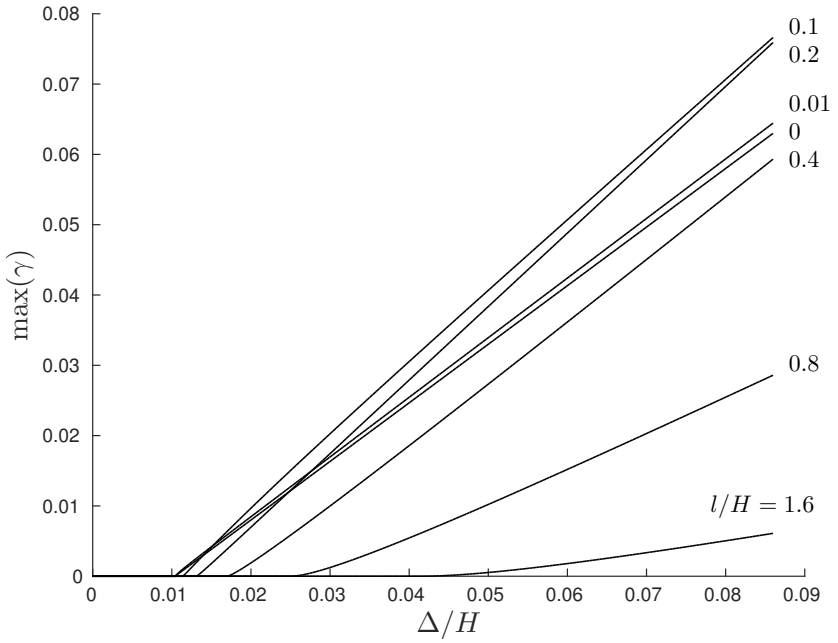

Figure 4: Slip profile amplitude to the imposed overall shear strain Δ/H for single slip ($\theta = 90°$), for various values of the normalized length parameter l/H. The normalized conventional strain hardening parameter is $h/G = 0.2$.

In the interval of l/H between 0.4 and 0.8, very little change in the distribution is predicted. However, as l/H is increased from 0.8 the distribution is seen to decrease in value throughout the strip, with a distinctly different distribution compared to values of $l/H < 0.4$.

The effects associated with the conventional strain hardening parameter are presented in Figs. 7 - 9, for the normalized length parameter $l/H = 0.4$. Figure 7 displays the effect of varying h/G on the resolved shear stress response. The results clearly reflect a large change in hardening predictions, with $h/G = 5\times10^{-4}$ predicting an almost ideally plastic response. The conventional strain hardening parameter is seen to govern the hardening response, since no hardening is seen for $h/G = 5 \times 10^{-5}$ despite a non-zero value of the length parameter. However, the strengthening response is seen to be independent of the conventional strain hardening parameter as all curves in Fig. 7 transition to the elastic-plastic

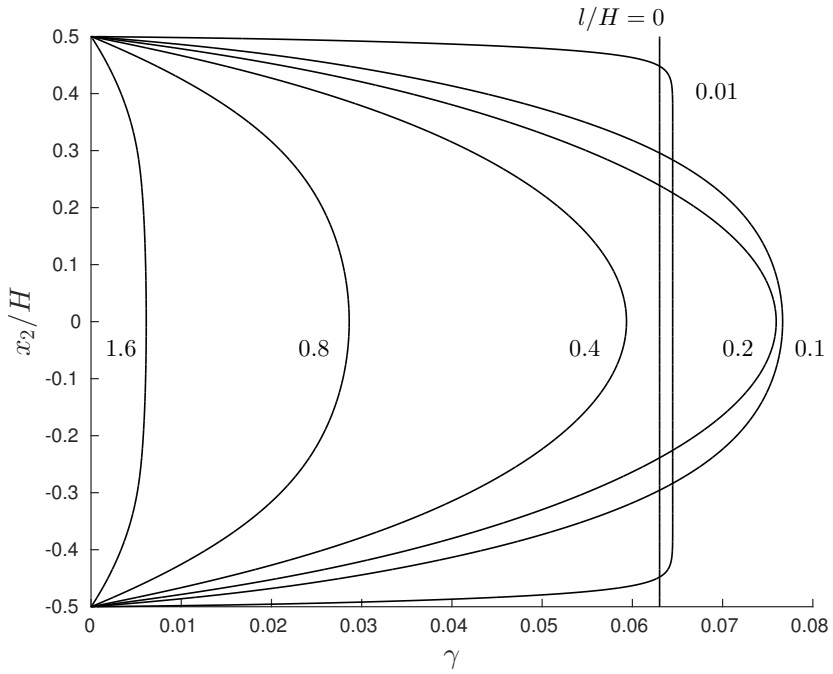

Figure 5: Slip profile, γ, at imposed overall shear strain $\Delta/H = 0.086$ for single slip ($\theta = 90°$), for various values of the normalized length parameter l/H. The normalized conventional strain hardening parameter is $h/G = 0.2$.

regime at the same resolved shear stress level. The relationship between the length parameter and both the strengthening response and the hardening slope are further investigated and discussed in Section 5.2. The effect of varying h/G on the slip profile distribution is shown in Fig. 8. The predicted slip profiles reflect the decrease in h/G through an overall increase in slip profile amplitude. The results obtained for $h/G = 5 \times 10^{-4}$ and $h/G = 5 \times 10^{-5}$ predict very sharp boundary layers in combination with a slight decrease in the slip profile amplitude, compared to the result for $h/G = 5 \times 10^{-3}$. The effect of conventional strain hardening on the slip profile is also examined by Bittencourt et al. (2003). Their results, which are obtained using a rate-independent strain gradient crystal plasticity formulation, similarly reveal that conventional strain hardening (slip system dissipative hardening in their terminology) has a strong

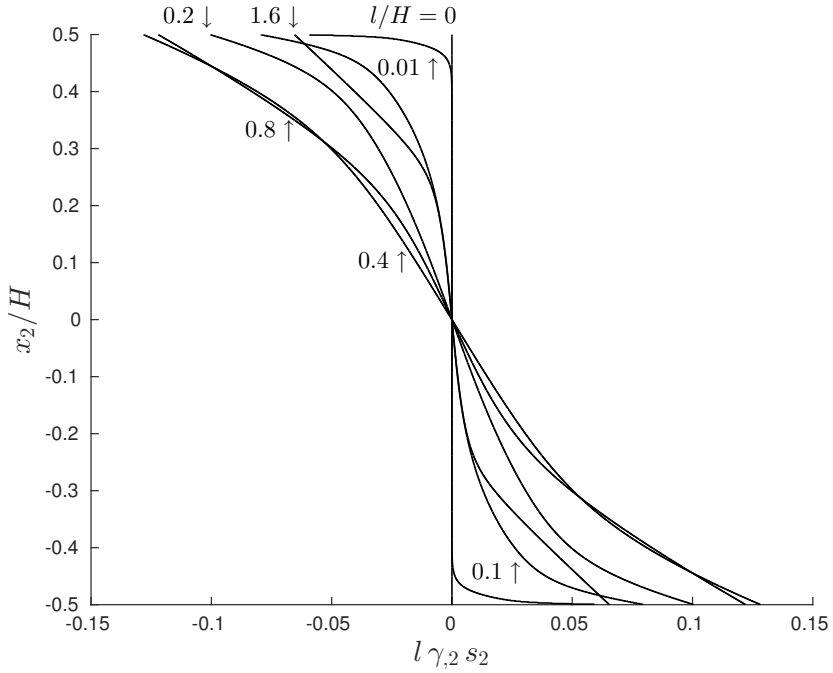

Figure 6: Normalized net Burgers vector density profile, $l\,\gamma_{,2}\,s_2$, at imposed overall shear strain $\Delta/H = 0.086$ for single slip ($\theta = 90°$), for various values of the normalized length parameter l/H. The normalized conventional strain hardening parameter is $h/G = 0.2$.

effect on the slip profile distribution for the case of pure shear loading. Figure 9 shows the normalized net Burgers vector density predictions associated with the slip profiles in Fig. 8. The data plotted is restricted to the interval between $l\,\gamma_{,2}\,s_2 = -0.5$ and $l\,\gamma_{,2}\,s_2 = 0.5$, such that a visual comparison is possible. The cut-off interval excludes determination of the peak values for $h/G = 5 \times 10^{-4}$ and $h/G = 5 \times 10^{-5}$, which are 1.432 and 3.932, respectively. The distribution is seen to increase near the boundaries for decreasing values of h/G, with a very sharp peak predicted for values of $h/G \leq 5 \times 10^{-3}$. Furthermore, an overall decrease in magnitude is predicted away from the boundaries for these low values of h/G. A comparison of the normalized net Burgers vector density profiles associated with various values of l/H and h/G (Fig. 6 and Fig. 9) indicates that a highly localized distribution is predicted at the boundaries for low values

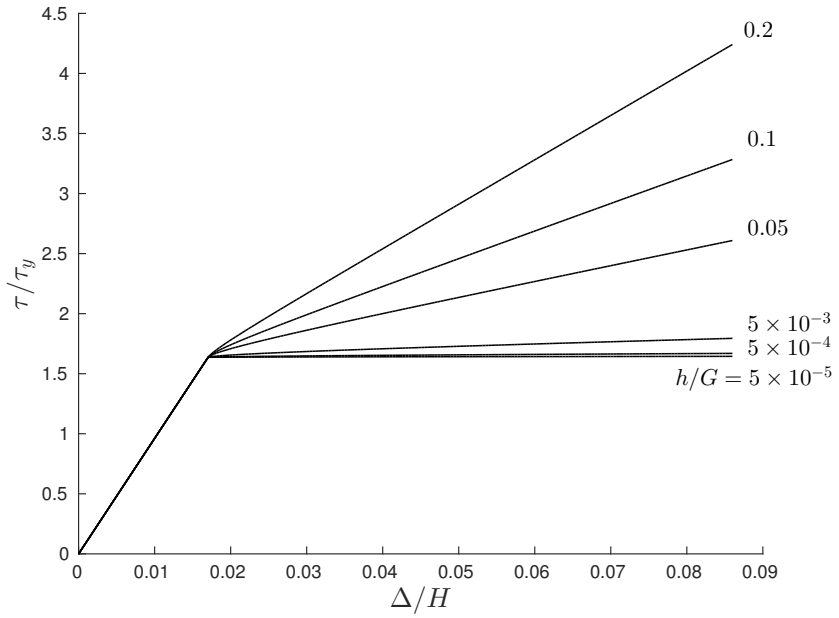

Figure 7: Shear stress response to the imposed overall shear strain Δ/H for single slip ($\theta = 90°$), for various values of the normalized conventional strain hardening parameter h/G. The value of normalized length parameter is $l/H = 0.4$.

of both length parameter and conventional strain hardening parameter.

5.2. Comparison between single slip and double slip

The strengthening and hardening characteristics for different slip system orientations are comparable through relatively simple relationships. To illustrate these relationships the average slip is defined by $\bar{\gamma} = \frac{1}{H}\int_{-H/2}^{H/2} \gamma[x_2]\mathrm{d}x_2$ and a normalized length parameter by $2\, l_\theta s_{2\theta}/H$. The slip direction vector component $s_{2\theta}$ is constant for a given choice of slip system orientation and l_θ is the slip system orientation dependent length parameter. Furthermore, it is noted that any discussion of the slip system orientation $\theta = 90°$ only refers to single slip and all other values of θ refers to symmetric double slip.

The resolved shear stress on the two slip systems for the pure shear problem is given by; $\tau = 2\,\sigma_{12}\,\mu_{12\theta}$, where the Schmid orientation tensor component, $\mu_{12\theta}$, depends on the slip system orientation (see Eq. (1)). Thus, for compar-

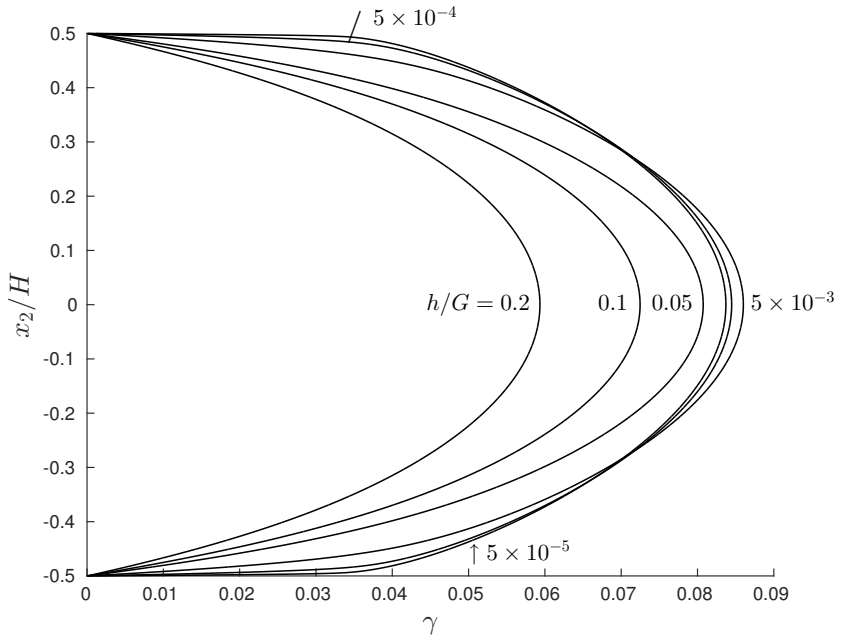

Figure 8: Slip profile, γ, at imposed overall shear strain $\Delta/H = 0.086$ for single slip ($\theta = 90°$), for various values of the normalized conventional strain hardening parameter h/G. The value of normalized length parameter is $l/H = 0.4$.

ison of results (between single slip and symmetric double slip), strengthening predictions are shown in Fig. 10 using the slip system orientation specific normalized resolved shear stress expression $\tau/(2\,\tau_y\,\mu_{12\theta})$. The figure shows the slip system specific normalized resolved shear stress as a function of the average slip for three slip system orientations ($\theta = 15°$, $30°$ and $90°$, respectively) and two values of normalized length parameter, $2\,l_\theta s_{2\theta}/H = 0.5$ and 1. It is seen that the chosen normalization of the resolved shear stress, predicts comparable strengthening which is dependent on the value of the normalized length parameter. The hardening predictions are not comparable using the chosen normalization, but by plotting the results using the normalized resolved shear stress τ/h the hardening predictions become comparable and dependent only on the normalized length parameter. Predictions of strengthening are shown in Fig. 11 for a wide range of length parameters. In the case of the present theory, the

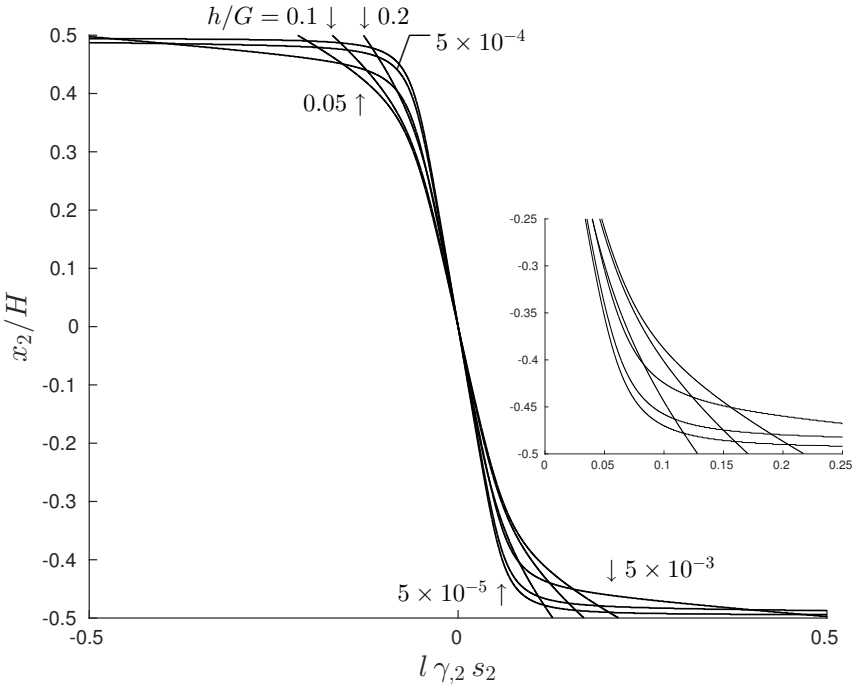

Figure 9: Normalized net Burgers vector density profile, $l\,\gamma_{,2}\,s_2$, at imposed overall shear strain $\Delta/H = 0.086$ for single slip ($\theta = 90°$), for various values of the normalized conventional strain hardening parameter h/G. The value of normalized length parameter is $l/H = 0.4$. A zoom of the results near the lower boundary is included.

results are obtained using one specific conventional strain hardening parameter ($h/G = 0.2$), but it has been confirmed to be independent of h/G. Hence, the predicted strengthening is independent of conventional strain hardening. Three sets of markers representing discrete data points, for the slip system orientations ($\theta = 15°$, $30°$ and $90°$, respectively) are plotted together with dashed lines which are linear interpolations between points. Two additional sets of markers are included, one set is obtained with the rate-dependent isotropic strain gradient plasticity theory proposed by Gudmundson (2004) and investigated by Niordson and Legarth (2010) and the other set is presented in Fleck et al. (2015). The predictions of Niordson and Legarth (2010) are obtained for an elastic-perfectly plastic material under pure shear loading and show strength-

ening (increase in effective yield strength in their terminology) as a function of a normalized dissipative length parameter. These results plotted in Fig. 11, are scaled by a factor of $2/\sqrt{3}$ on the normalized length parameter axis to allow for a direct comparison with the results of the present theory. The scaling factor is necessary due to the definition of the effective plastic strain measure in the theory proposed by Gudmundson (2004), which is defined without the Mises strain factor of 2/3. Furthermore, the results of Niordson and Legarth (2010) are representative of the rate-dependent strain gradient crystal plasticity formulation presented by Niordson and Kysar (2014). The strengthening predictions of Fleck et al. (2015) are obtained for the case of tensile stretching of a plastically passivated layer, using a power law relation for plasticity, and they present strengthening (elastic loading gap in their terminology) as a function of a normalized recoverable length parameter. A scaling of the results is unnecessary due to the definition of the effective strain measure in Fleck et al. (2015). Furthermore, their results are obtained using a formulation which is closely related to the formulation presented by Hutchinson (2012). Common to all results plotted in Fig. 11 is a slow increase in strengthening for small values of length parameter, while an almost linear relationship is predicted for larger values of the length parameter. However, while the results of Fleck et al. (2015) are almost qualitatively equivalent to the results of the present theory, a qualitative difference is seen in the results of Niordson and Legarth (2010).

Figure 12 presents the normalized average effective hardening modulus, $h_{eff}/h = (\tau - \tau_y)/(\bar{\gamma}h)$, as a function of normalized length parameter. Due to a slight initial curvature of the response curves (similar to those seen in Fig. 10) the effective hardening modulus is calculated using data points at 90 % and 100 % of the imposed overall shear strain. The data plotted is obtained using the normalized conventional strain hardening parameter ($h/G = 0.2$), but results have been shown to be independent of non-zero values of h/G. The markers on the curve are discrete data points, for three values of slip system orientation ($\theta = 15^\circ$, 30° and 90°, respectively), and the solid line is plotted using a fitted second order polynomial; $2.6110\,(2\,l_\theta s_{2\theta}/H)^2 + 0.5773\,(2\,l_\theta s_{2\theta}/H) + 1.0$. The

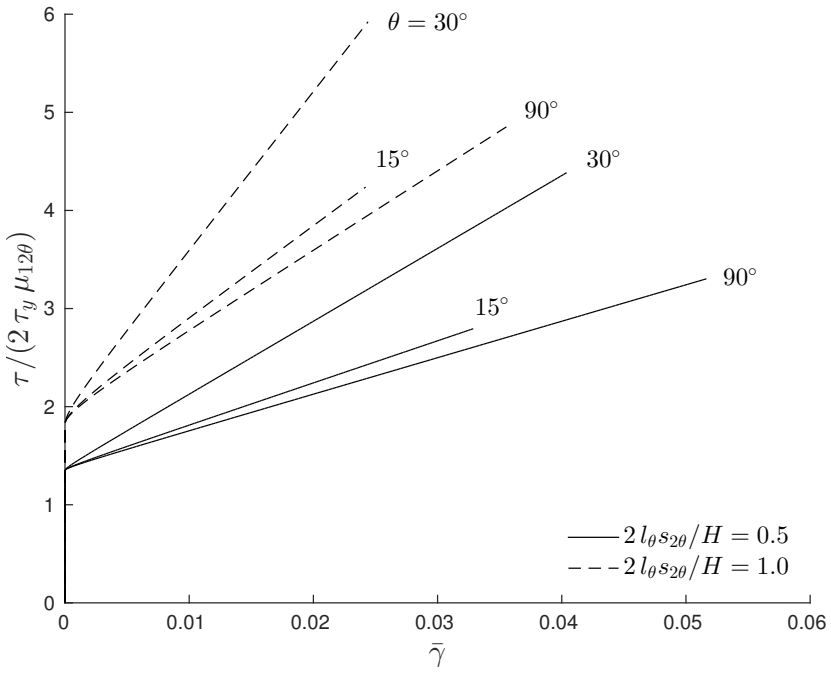

Figure 10: Slip system dependent normalized resolved shear stress as a function of average slip. The choice of normalization captures the equivalent strengthening for three different slip system orientations ($\theta = 15°, 30°$ and $90°$, respectively) at two different values of normalized length parameter $2\,l_\theta s_{2\theta}/H$.

coefficient of determination for the fitted polynomial is $R^2 = 0.9966$. Niordson and Legarth (2010) investigated the effective hardening modulus as a function of their energetic length parameter and obtained a quadratic relationship (similar to Fig. 12, but with a vanishing linear term). Furthermore, their results are supported by an analytical expression based on a rate-independent and perfectly plastic material behavior.

6. Concluding remarks

An extension of the conventional rate-independent crystal plasticity framework, which incorporates gradient of slip has been presented. The extension builds on the underlying ideas by Hutchinson (2012) of extending conventional

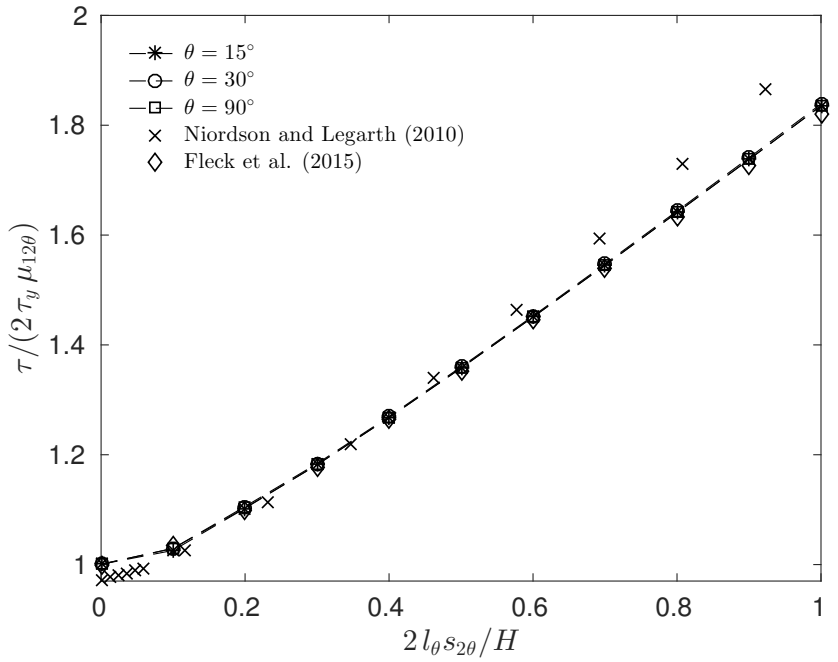

Figure 11: Effect of normalized length parameter $2\,l_\theta s_{2\theta}/H$ on strengthening predictions. Points represent solution values obtained numerically for three different slip system orientations ($\theta = 15°, 30°$ and $90°$, respectively), while the dashed lines are linear interpolations between points. Furthermore, points representing solution values obtained by Niordson and Legarth (2010) and Fleck et al. (2015) are also included.

isotropic J_2-theory to account for strain gradient effects. Following Hutchinson (2012) three objectives related to the extension are defined. The first objective has been highlighted through the single slip results, where the theory has been shown to reduce to the conventional crystal plasticity framework in the limit $l \to 0$. The second objective is enforced throughout the presented theory by restricting parameters that govern material behavior to the shear modulus, Poisson's ratio, a hardening relation between resolved shear stress and slip, and a material length parameter that scales the gradient effect. This objective defines the main assumption that is used to govern the evolution of plastic flow, which is incorporated by relating the gradient enhanced effective plastic strain measure to a shear relation between resolved shear stress and slip in the plastic

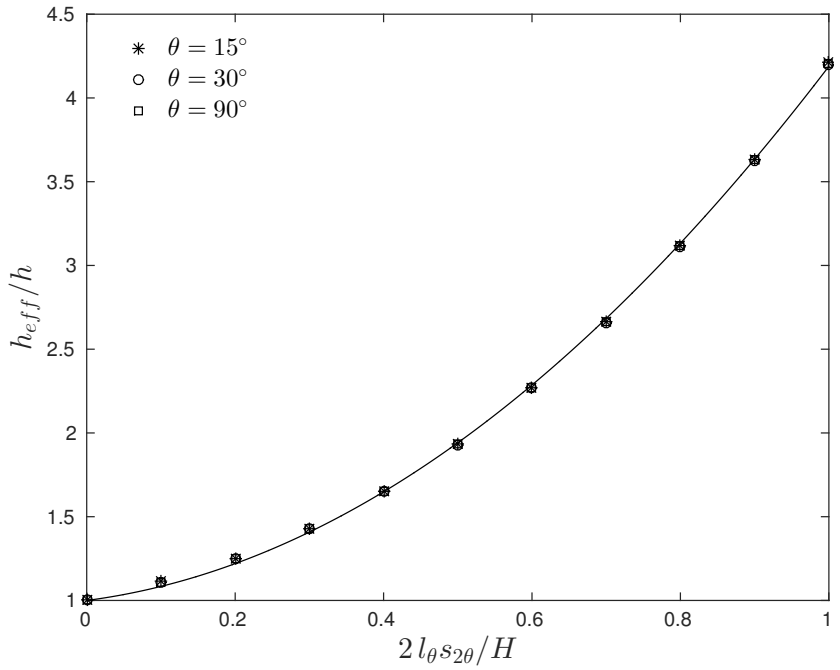

Figure 12: Effect of normalized length parameter $2\,l_\theta s_2/H$ on the normalized average effective hardening moduli $h_{eff}/h = (\tau - \tau_y)/(\bar{\gamma} h)$, for three different values of slip system orientation angle ($\theta = 15^\circ, 30^\circ$ and 90°, respectively), and the value of the normalized conventional strain hardening parameter is $h/G = 0.2$. The solid line is a fitted second order polynomial given by; $2.6110\ (2\,l_\theta s_{2\theta}/H)^2 + 0.5773\ (2\,l_\theta s_{2\theta}/H) + 1.0$, with the coefficient of determination for the fitted polynomial: $R^2 = 0.9966$.

regime. The shear relation must increase monotonically, and no further restrictions on the hardening law exist in the framework presented. The present work takes as offset linear hardening, but more complex hardening laws could readily be incorporated into the formulation. The definition of the plastic work is in the present formulation based on the assumption that the work related to gradients of slip is recoverable, while the work related to slip is a combination of both dissipative and recoverable energy contributions. The present theory relates the effective strain to both terms of the shear hardening curve, and this is of critical importance to the strengthening predictions of the present theory, as discussed by Fleck et al. (2015) for isotropic plasticity. The third objective by Hutchin-

son (2012) states that flow theory and deformation theory must coincidence in the case of proportional straining history. This objective is not fulfilled for the examined problem of pure shear loading where a slightly non-proportional straining is predicted (see Fig. 4). However, the overall trends of the results seem to indicate that model predictions converge towards proportional straining in the plastic regime as the effects due to strengthening become negligible.

The incremental formulation presented is derived based on an assumption of monotonic loading to simplify the implementation procedure, while preserving the characteristics of strengthening and hardening behavior. The results of single slip in the case of pure shear loading are used to quantify these characteristics. Strengthening is shown to increase for increasing values of the length parameter, while it is predicted to be independent of the conventional strain hardening parameter. The distribution of slip is shown to depend on both the conventional strain hardening parameter and the length parameter, such that a concentration in the net Burgers vector density is predicted at the boundaries for low values of either the length parameter or the conventional strain hardening parameter. Predictions similar to these have recently been the focus of an investigation performed by El-Naaman et al. (2016). Their findings relate these slip gradient distributions to experimentally observed dislocation arrangements of individual grains of crystalline materials, known as wall and cell structures.

Slip system dependent strengthening and hardening predictions of the model is also presented in the present work. Two slip systems oriented symmetrically with respect the x_1-axis (see Fig. 2) predict results comparable to those of single slip. The normalized length parameter $2\,l_\theta s_{2\theta}/H$ is shown to characterize both strengthening and hardening predictions. Results are compared to the isotopic strain gradient formulation investigated in Niordson and Legarth (2010) (equal results would be predicted by the crystal plasticity formulation investigated in Niordson and Kysar, 2014), and despite several differences between the formulations strengthening and hardening predictions show similar trends. Furthermore, model predictions of the strengthening behavior are almost qualitatively equivalent to the recent findings of Fleck et al. (2015).

Lastly, the monotonic loading assumption excludes investigation of unloading and reverse loading. Recently the work of Liu et al. (2015) which presents cyclic torsion experiments of micron diameter copper and gold wires has revealed size dependent strengthening and a Bauschinger effect. In light of these results, a very interesting extension of the present model is the case of general loading, which would permit investigation of strengthening and hardening characteristics of unloading and cyclic loading.

7. Acknowledgements

The authors are grateful for fruitful discussions with Professor John W. Hutchinson related to the model development and interpretation of the results. This work is financially supported by The Danish Council for Independent Research under the research career program Sapere Aude. Grant 11-105098, "*Higher Order Theories in Solid Mechanics*".

Appendix A.

In Section 2 the derivatives $\frac{\partial|\gamma^{(\alpha)}|}{\partial\gamma^{(\alpha)}} = \text{sgn}[\gamma^{(\alpha)}]$, for $\gamma^{(\alpha)} \neq 0$ and $\frac{\partial\gamma^{(\alpha)}_{acc}}{\partial\gamma^{(\alpha)}} = \text{sgn}[\dot{\gamma}^{(\alpha)}]$, for $\dot{\gamma}^{(\alpha)} \neq 0$ are defined, where sgn[$*$] denotes the sign function. This appendix presents and discusses details related to the evolution of these derivatives and the slip measures $\gamma^{(\alpha)}$, $|\gamma^{(\alpha)}|$ and $\gamma^{(\alpha)}_{acc}$ through a general loading history. The evolution of the slip is given by $\gamma^{(\alpha)} = \int_0^t \dot{\gamma}^{(\alpha)} \mathrm{d}t'$, while the evolution of the slip related to conventional strain hardening (the monotonicaly increasing slip measure) follows the accumulated slip defined in the rate-dependent theory presented by Kuroda and Tvergaard (2006). Thus, the accumulated slip measure is given by; $\gamma^{(\alpha)}_{acc} = \int_0^t |\dot{\gamma}^{(\alpha)}| \mathrm{d}t'$, which is used to account for the total plastic slip throughout a general loading history. The presented theory defines the slip as being work conjugate to the micro-stress, as is the case for conventional rate-independent crystal plasticity where Eq. (10) simplifies to $q^{D(\alpha)} = \tau^{(\alpha)}$ (as discussed in Section 2). Thus, the two derivatives are needed

to derive the micro-stress under a general loading history (given by Eq. (14)). The superscript (α) is omitted in the remainder of this appendix.

In Fig. A.13 a graphical interpretation of the derivatives are given based on the evolution of the slip increment, $\dot{\gamma}$, and the slip measures γ, $|\gamma|$ and γ_{acc}. The loading history varies according to Fig. A.13 **(a)**, otherwise the details leading to the evolution of the plastic deformation are undefined. Figure A.13 **(a)** shows the $\dot{\gamma}$ axis with the evolution of slip increment given by the (pseudo time) increments t_i. The evolution of the slip through the increments t_i are shown in Fig. A.13 **(b)** and **(c)**, versus $|\gamma|$ and γ_{acc}, respectively. Initial yield occurs at the increment leading up to t_1, such that $\dot{\gamma}[t_1] = \gamma[t_1] = |\gamma|[t_1] = \gamma_{acc}[t_1] = 1$. The following increment results in $\dot{\gamma}[t_2] = 2$ and $\gamma[t_2] = |\gamma|[t_2] = \gamma_{acc}[t_2] = 3$. The increment t_3 results in $\dot{\gamma}[t_3] = 1$ and $\gamma[t_3] = |\gamma|[t_3] = \gamma_{acc}[t_3] = 4$, thus, the derivatives evaluated in the interval t_1 to t_3 are $\frac{\partial|\gamma|}{\partial\gamma} = \frac{\partial\gamma_{acc}}{\partial\gamma} = \text{sgn}[\gamma] = \text{sgn}[\dot{\gamma}] = 1$. The following increment results in $\dot{\gamma}[t_4] = 0$ (i.e. no plastic deformation), thus, $\gamma[t_4] = |\gamma|[t_4] = \gamma_{acc}[t_4] = 4$ and $\frac{\partial|\gamma|}{\partial\gamma} = \text{sgn}[\gamma] = 1$, but $\frac{\partial\gamma_{acc}}{\partial\gamma}$ is undefined since $\dot{\gamma}[t_4] = 0$. However, since no plastic deformation has occurred no change in the micro-stress arises, and the value of the derivative $\frac{\partial\gamma_{acc}}{\partial\gamma}$ is not needed. The following increment results in $\dot{\gamma}[t_5] = -1$, with $\gamma[t_5] = |\gamma|[t_5] = 3$ and $\gamma_{acc}[t_5] = 5$, thus, reversal of the sign of the load results in $\frac{\partial|\gamma|}{\partial\gamma} = \text{sgn}[\gamma] = 1$ and $\frac{\partial\gamma_{acc}}{\partial\gamma} = -1$. The increment t_6 results in $\dot{\gamma}[t_6] = -2$, with $\gamma[t_6] = |\gamma|[t_6] = 1$ and $\gamma_{acc}[t_6] = 7$. The following increment results in $\dot{\gamma}[t_7] = -1$, with $\gamma[t_7] = |\gamma|[t_7] = 0$ and $\gamma_{acc}[t_7] = 8$. As seen γ and $|\gamma|$ retain no information about the previous loading at this stage of the deformation, while γ_{acc} accounts for the previous loading history. The derivative $\frac{\partial\gamma_{acc}}{\partial\gamma} = \text{sgn}[\dot{\gamma}] = -1$, while the derivative $\frac{\partial|\gamma|}{\partial\gamma}$ is undefined since $\gamma[t_7] = 0$. However, viewed from a numerical point of view, it will be practically impossible to encounter the exact value of $\gamma = 0$. The increment t_8 results in $\dot{\gamma}[t_8] = -2$, with $\gamma[t_8] = -2$, $|\gamma|[t_8] = 2$, $\gamma_{acc}[t_8] = 10$, $\frac{\partial|\gamma|}{\partial\gamma} = \text{sgn}[\gamma] = -1$ and $\frac{\partial\gamma_{acc}}{\partial\gamma} = \text{sgn}[\dot{\gamma}] = -1$. The following increment results in $\dot{\gamma}[t_9] = 0$, thus, $\gamma[t_9] = -2$, $|\gamma|[t_9] = 2$, $\gamma_{acc}[t_9] = 10$, $\frac{\partial|\gamma|}{\partial\gamma} = \text{sgn}[\gamma] = -1$ and $\frac{\partial\gamma_{acc}}{\partial\gamma}$ is undefined. Lastly, the increment t_{10} results in $\dot{\gamma}[t_{10}] = 1$, with $\gamma[t_{10}] = -1$, $|\gamma|[t_{10}] = 1$, $\gamma_{acc}[t_{10}] = 11$, $\frac{\partial|\gamma|}{\partial\gamma} = \text{sgn}[\gamma] = -1$ and

$\frac{\partial \gamma_{acc}}{\partial \gamma} = \text{sgn}[\dot{\gamma}] = 1$. From this example it is evident that sgn$[\gamma]$ and sgn$[\dot{\gamma}]$ are equal when γ increases in magnitude (when $|\gamma|$ increases in value), while they are opposite in sign when γ decreases in magnitude. The derivative $\frac{\partial |\gamma|}{\partial \gamma}$ is undefined in the case of $\gamma = 0$ and $\frac{\partial \gamma_{acc}}{\partial \gamma}$ is undefined in the case of $\dot{\gamma} = 0$, however, the practical consequences of the derivatives being undefined at certain instances during a general loading are shown to be negligible. Furthermore, while the derivative $\frac{\partial \gamma_{acc}}{\partial \gamma} = \text{sgn}[\dot{\gamma}]$ is governed by $\dot{\gamma}$ the evolution of γ_{acc} depends on the evolution of the slip γ, as is the case of the slip measure $|\gamma|$ and its derivative $\frac{\partial |\gamma|}{\partial \gamma}$. Thus, only the micro-stress measure related to conventional rate-independent crystal plasticity theory, $q^{D(\alpha)}$, depends on the slip increment.

Appendix B.

In section 3 the existence of initially (at the onset of yield) unbounded terms of the stiffness matrix is noted. Thus, a numerical solution is not available when $\gamma = 0$ at initial yield. To overcome this issue, results presented in the present work are obtained using a small initial value of the slip; $\gamma = \gamma_{eff} = \omega[l/H]\,\gamma_y$, which is defined in terms of the yield strain, γ_y, and the scaling parameter, $\omega[l/H]$. Figure B.14 presents the influence of $\omega[l/H]$ on the deviation between slip profile amplitudes at the final stage of deformation. The slip profile amplitude is defined as $A[\omega[l/H]] = \max(\gamma[\omega[l/H]])$ and the deviation in % between the slip profile amplitude and a reference value of the slip profile amplitude, $A[\omega_o[l/H]]$, is determined by $\frac{A[\omega[l/H]] - A[\omega_o[l/H]]}{A[\omega_o[l/H]]}\,100\%$. Here, $\omega_o[l/H]$ refers to the lowest possible values at which a numerical solution is obtained for that specific normalized length parameter. Results are presented for the case of single slip ($\theta = 90^\circ$) with $\gamma_y = \tau_y/G = 0.0104$ for three choice of normalized length parameter $l/H = 0.1, 0.8$, and 1.6, using the normalized conventional strain hardening parameter $h/G = 0.2$. The markers on the curves represent discrete data values, solid lines are linear interpolations between points, while the dashed line indicates the value of $\omega[l/H]$ (being 2×10^{-3}) used to obtain the results presented in Figs. 3 - 12. Figure B.14 shows that for increasing values of

l/H a solution can be obtained for decreasing values of $\omega[l/H]$, with the difference between $\omega[0.1]$ and $\omega[1.6]$ being above an order of magnitude. The lowest possible values are obtained using $\omega_o[0.1] = 2 \times 10^{-6}, \omega_o[0.8] = 7 \times 10^{-6}$, and $\omega_o[1.6] = 7 \times 10^{-5}$, respectively. Furthermore, as seen the deviation increases for increasing values of l/H at a specific value of $\omega[l/H]$. The largest deviation in the slip profile amplitude is below 1 % for $\omega = 2 \times 10^{-3}$ (corresponding to the initialization value $\gamma_{eff} = 2.08 \times 10^{-5}$), confirming that this value leads to reasonable precision for the slip system orientation angle $\theta = 90°$. The presented theory is phenomenologically based, however, it is worth mentioning that Eq. (2), and the relation for the net Burgers vector density $\rho_{GND} b = \gamma^{(\alpha)}_{,i} s^{(\alpha)}_i$, leads to a $\gamma^{(\alpha)}_{eff} = 10^{-3}$, when using the material parameters; an initial dislocation density of a single crystal $\rho \sim 10^{12}$ m^{-2}, a Burgers vector magnitude of $b \sim 10^{-9}$ m and a material length parameter of $l \sim 10^{-6}$ m, which are all within an order of magnitude of regularly reported values.

References

Balay, S., Abhyankar, S., Adams, M.F., Brown, J., Brune, P., Buschelman, K., Dalcin, L., Eijkhout, V., Gropp, W.D., Kaushik, D., Knepley, M.G., McInnes, L.C., Rupp, K., Smith, B.F., Zampini, S., Zhang, H., 2015. PETSc Users Manual. Technical Report ANL-95/11 - Revision 3.6. Argonne National Laboratory. URL: http://www.mcs.anl.gov/petsc.

Bardella, L., 2006. A deformation theory of strain gradient crystal plasticity that accounts for geometrically necessary dislocations. Journal of the Mechanics and Physics of Solids 54, 128 – 160. doi:http://dx.doi.org/10.1016/j.jmps.2005.08.003.

Bittencourt, E., Needleman, A., Gurtin, M., der Giessen, E.V., 2003. A comparison of nonlocal continuum and discrete dislocation plasticity predictions. Journal of the Mechanics and Physics of Solids 51, 281 – 310. doi:http://dx.doi.org/10.1016/S0022-5096(02)00081-9.

Borg, U., 2007. Strain gradient crystal plasticity effects on flow localization. International Journal of Plasticity 23, 1400 – 1416. doi:http://dx.doi.org/10.1016/j.ijplas.2007.01.003.

Davis, T., Duff, I., Amestoy, P., Gilbert, J., Larimore, S., Natarajan, E.P., Chen, Y., W, H., Rajamanickam, S., 2014. SuiteSparse: a suite of sparse matrix packages. http://faculty.cse.tamu.edu/davis/suitesparse.html.

El-Naaman, S., Nielsen, K., Niordson, C., 2016. On modeling micro-structural evolution using a higher order strain gradient continuum theory. International Journal of Plasticity 76, 285 – 298. doi:http://dx.doi.org/10.1016/j.ijplas.2015.08.008.

Fleck, N., Muller, G., Ashby, M., Hutchinson, J., 1994. Strain gradient plasticity: Theory and experiment. Acta Metallurgica et Materialia 42, 475 – 487. doi:http://dx.doi.org/10.1016/0956-7151(94)90502-9.

Fleck, N., Willis, J., 2009. A mathematical basis for strain-gradient plasticity theorypart i: Scalar plastic multiplier. Journal of the Mechanics and Physics of Solids 57, 161 – 177. doi:http://dx.doi.org/10.1016/j.jmps.2008.09.010.

Fleck, N.A., Hutchinson, J.W., Willis, J.R., 2014. Strain gradient plasticity under non-proportional loading, in: Proceedings of the Royal Society of London A: Mathematical, Physical and Engineering Sciences, The Royal Society. p. 20140267.

Fleck, N.A., Hutchinson, J.W., Willis, J.R., 2015. Guidelines for constructing strain gradient plasticity theories. Journal of Applied Mechanics 82. doi:10.1115/1.4030323.

Gudmundson, P., 2004. A unified treatment of strain gradient plasticity. Journal of the Mechanics and Physics of Solids 52, 1379 – 1406. doi:http://dx.doi.org/10.1016/j.jmps.2003.11.002.

Gurtin, M.E., 2000. On the plasticity of single crystals: free energy, microforces, plastic-strain gradients. Journal of the Mechanics and Physics of Solids 48, 989 – 1036. doi:http://dx.doi.org/10.1016/S0022-5096(99)00059-9.

Gurtin, M.E., 2002. A gradient theory of single-crystal viscoplasticity that accounts for geometrically necessary dislocations. Journal of the Mechanics and Physics of Solids 50, 5 – 32. doi:http://dx.doi.org/10.1016/S0022-5096(01)00104-1.

Gurtin, M.E., Anand, L., Lele, S.P., 2007. Gradient single-crystal plasticity with free energy dependent on dislocation densities. Journal of the Mechanics and Physics of Solids 55, 1853 – 1878. doi:http://dx.doi.org/10.1016/j.jmps.2007.02.006.

Hutchinson, J., 2012. Generalizing J_2 flow theory: Fundamental issues in strain gradient plasticity. Acta Mechanica Sinica 28, 1078–1086. doi:10.1007/s10409-012-0089-4.

Kuroda, M., Tvergaard, V., 2006. Studies of scale dependent crystal viscoplasticity models. Journal of the Mechanics and Physics of Solids 54, 1789 – 1810. doi:http://dx.doi.org/10.1016/j.jmps.2006.04.002.

Liu, D., He, Y., Shen, L., Lei, J., Guo, S., Peng, K., 2015. Accounting for the recoverable plasticity and size effect in the cyclic torsion of thin metallic wires using strain gradient plasticity. Materials Science and Engineering: A 647, 84 – 90. doi:http://dx.doi.org/10.1016/j.msea.2015.08.063.

Niordson, C., Kysar, J., 2014. Computational strain gradient crystal plasticity. Journal of the Mechanics and Physics of Solids 62, 31–47. doi:10.1016/j.jmps.2013.08.014.

Niordson, C.F., Legarth, B.N., 2010. Strain gradient effects on cyclic plasticity. Journal of the Mechanics and Physics of Solids 58, 542 – 557. doi:10.1016/j.jmps.2010.01.007.

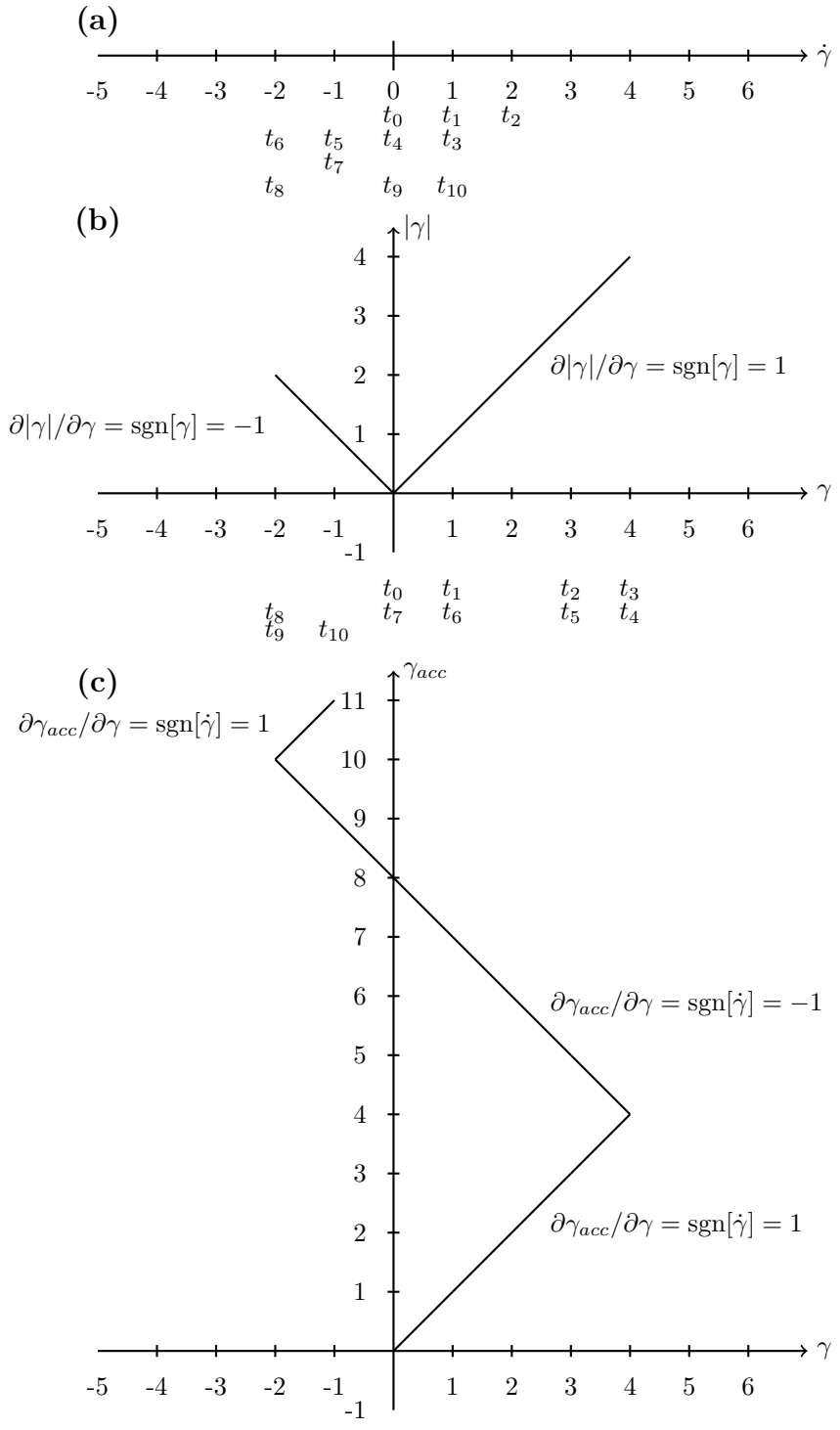

Figure A.13: Evolution of the plastic strain measures; $\dot{\gamma}$, γ, $|\gamma|$, γ_{acc} and the derivatives $\partial|\gamma|/\partial\gamma$ and $\partial\gamma_{acc}/\partial\gamma$ during a loading history from t_0 to t_{10}. **(a)** Shows the evolution of the slip increment $\dot{\gamma}$ during the loading history indicated below the $\dot{\gamma}$ axis. **(b)** Shows the absolute value of the slip versus the slip and the slope of the curves ($\partial|\gamma|/\partial\gamma$) during the loading history indicated below the γ axis. **(c)** Shows the accumulated slip versus the slip and the slope of the curves ($\partial\gamma_{acc}/\partial\gamma$) during the loading history indicated above the plot.

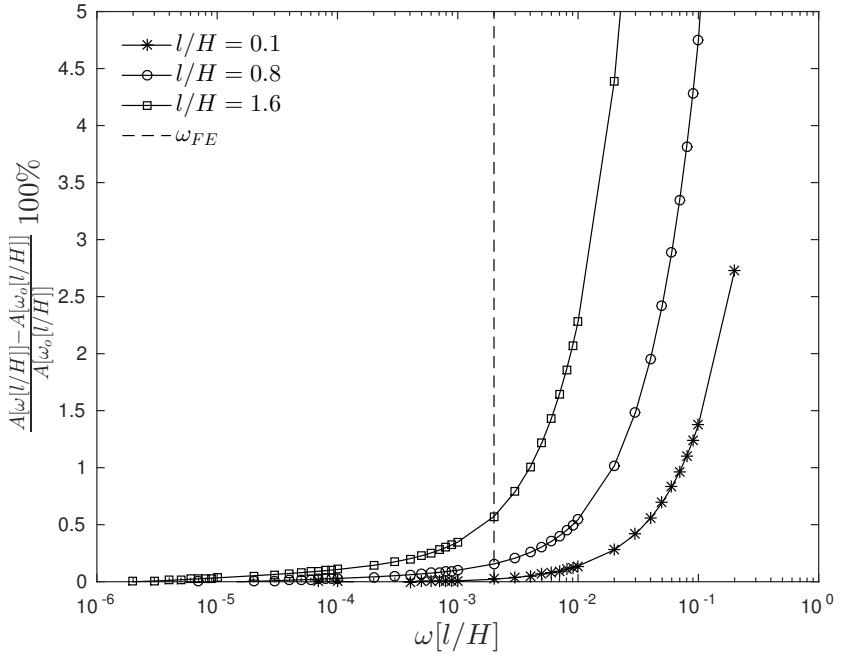

Figure B.14: Effect of initialization parameter $\omega[l/H]$ on the deviation in %, $\frac{A[\omega[l/H]]-A[\omega_o[l/H]]}{A[\omega_o[l/H]]}\,100\%$, of the slip profile amplitude, $A[\omega[l/H]]$, and a reference slip profile amplitude, $A[\omega_o[l/H]]$, at the prescribed overall shear strain value $\Delta/H = 0.086$. The results are obtained for the case of single slip ($\theta = 90^\circ$), for three values of the normalized length parameter $l/H = 0.1, 0.8$ and 1.6, and the conventional strain hardening parameter is $h/G = 0.2$. The dashed line indicates the value, $\omega_{FE} = 2 \times 10^{-3}$, which is used to obtain the results presented in Figs. 3 - 12.